Variational transition-state theory rate constant calculations with multidimensional tunneling corrections of the reaction of acetone with OH

Laura Masgrau, Àngels-González-Lafont* and José M. Lluch

Departament de Química, Universitat Autónoma de Barcelona, 08193 Bellaterra, Barcelona, Spain

Abstract

In this paper the first variational transition-state rate constant calculation for the OH + $CH_3COCH_3 \rightarrow$ P reaction is presented. The potential energy surface has been described by low level calculations at the B3LYP/6-31G* level combined with higher level calculations using the multilevel CBS-RAD technique. Three different reaction pathways have been found: abstraction of a H atom eclipsed to the carbonyl group of acetone, abstraction of a H atom alternated to the carbonyl group of acetone, and addition of the OH molecule to the carbon atom of the carbonyl group of acetone. To take into account the three different kinetic channels, the competitive canonical unified statistical theory has been used to calculate the global rate constant. However, in practice the global rate constant of the acetone + OH reaction turns out finally to be the sum of the eclipsed and alternated abstraction rate constants, leading to a clearly curved Arrhenius plot. The addition-elimination mechanism has an almost negligible contribution to the global rate constant at whatever temperature. The corresponding branching ratio is at most of ≈2% and attains even smaller values at the lowest temperature range.

1. Introduction

Although it has been recognized for many years that acetone is an important trace constituent of the troposphere, recent measurements have shown that concentration of acetone in the atmosphere is surprisingly high. Sources of acetone in the atmosphere are thought to be OH-initiated oxidation of some hydrocarbons, biogenic and anthropogenic emissions and biomass burning. Major sinks are photolysis and reaction with OH. The degradation of acetone in the troposphere leads to the formation of HO_x radicals and peroxy radicals (which through reaction with NO_2 form peroxyacetyl nitrate), in both cases resulting in increased ozone production.

The important role that acetone plays in troposphere chemistry has stimulated the study of the processes in which it intervenes. In particular, in the last recent years much research has been devoted to the kinetic studies of the reaction of acetone with the hydroxyl radical.[1-7] Unfortunately, significant discrepancies exist among the different reported results corresponding to this reaction, in such a way that a consistent mechanism is still lacking. This fact could seem surprising at first glance, but it has to be realized that the complete understanding of the reaction mechanism that governs a concrete atmospheric reaction is not an easy task at all even nowadays.

In 1987 the first measurement of the temperature dependence of the acetone + OH reaction rate was reported by Wallington and Kurylo,[1] who used the flash photolysis resonance fluorescence technique to monitor the OH radicals as a function of time at temperatures between 240 and 440 K. They obtained a linear Arrhenius plot with a bimolecular rate constant of $k(T) = (1.7 \pm 0.4) \times 10^{-12} \exp[-(600 \pm 75)/T]$ cm^3 molecule^{-1} s^{-1} which was attributed to the hydrogen atom abstraction process. Very similar results were obtained eleven years later by Mellouki and coworkers,[2] who followed the concentration of the OH radicals using the pulsed laser photolysis laser-induced fluorescence technique over the temperature range 243 - 372 K, obtaining the Arrhenius expression $k(T) = (1.25 \pm 0.22) \times 10^{-12} \exp[-(561 \pm 57)/T]$ cm^3 molecule^{-1} s^{-1}.

Very recently Crowley and coworkers[3] have extended the temperature-range of the kinetic data down to that typical of the upper troposphere. They have used pulsed laser photolysis generation of OH combined with both resonance fluorescence and pulsed laser-induced fluorescence detection between 202 and 395 K. Surprisingly the Arrhenius plot that they have obtained involves an important curvature (even negative temperature dependence below 240 K) which results in a significantly higher rate constant at low temperatures than obtained by extrapolation of the previous measurements, thus implying a greater significance for the reaction with OH as a sink for acetone in the upper troposphere. So, their kinetic data were not fitted using any single Arrhenius expression but the double equation

k(T) = (8.8 ± 3.6) x 10^{-12} exp [-(1320 ± 163)/T] + (1.7 ± 0.9) x 10^{-14} exp [(423 ± 109)/T] cm^3 molecule^{-1} s^{-1}. To explain this temperature dependence the authors have hypothesized that the overall reaction

$$OH + CH_3C(O)CH_3 \rightarrow products \qquad (R1)$$

proceeds mainly via hydrogen atom abstraction producing acetonyl radical at higher temperatures

$$OH + CH_3C(O)CH_3 \rightarrow H_2O + CH_3C(O)CH_2 \qquad (R1a)$$

while below room temperature electrophillic OH-addition to the carbonyl C atom followed by methyl elimination would dominate

$$OH + CH_3C(O)CH_3 \rightarrow (CH_3)_2C(O)OH \rightarrow CH_3 + CH_3COOH \qquad (R1b)$$
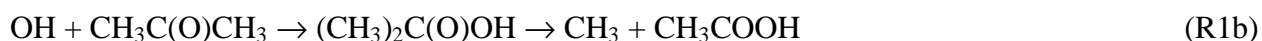
The contributions of the two channels would be roughly equal at 280 K. The hydrogen abstraction and the addition-elimination pathways would be responsible of the first and the second term (which involves a negative activation energy), respectively, in the double Arrhenius equation. In an additional paper, Wollenhaupt and Crowley[4] have presented an estimation of the branching ratio k_{1b}/k_1 , obtained by scavenging any CH_3 formed with NO_2 to generate CH_3O, which was detected by pulsed laser induced fluorescence. That branching ratio turned out to be 0.5 ± 0.15 and 0.3 ± 0.1 at 297 and 233 K, respectively. A few months later, Dóbé, Henon and coworkers,[6] using discharge-flow experiments, have determined a branching ratio k_{1a}/k_1 of 0.50 ± 0.04 at 298 K, so clearly supporting the results of Wollenhaupt and Crowley.[4] However, ab initio calculations also carried out by Dóbé, Henon and coworkers[6] at the CCSD(T)/6-311G(d,p)//MP2/6-31G(d,p) level introduce some elements of doubt. In effect, they have found that the hydrogen abstraction process occurs through a six-membered ring-like hydrogen bridged complex (already found by Aloisio and Francisco[8] at the B3LYP/6-31++G(3df,3pd) level) and a transition state structure that involves an energy barrier, including zero-point energy corrections, of 3.99 kcal/mol. In turn, the addition-elimination pathway takes place via a four-membered ring-like hydrogen bridged complex and a transition state structure with an energy barrier of 8.10 kcal/mol. It is clear that the size of this last positive energy barrier is clearly inconsistent with the experimental negative activation energy attributed to this channel.

Finally, new experiments by Peeters and coworkers[7] using a multi-stage fast-flow reactor and a molecular beam sampling mass spectrometry apparatus have introduced new elements of discrepancy. These authors have found no significant production of acetic acid at 290 K, resulting in a branching ratio $k_{1b}/k_1 \leq 0.03$. In addition, from the theoretical point of view, the same authors have found three pathways in the potential energy surface (PES) for the acetone + OH reaction: direct OH-addition plus CH_3 elimination, direct hydrogen abstraction, and formation of a six-membered ring-like hydrogen bridged complex followed by hydrogen abstraction. The

corresponding energy barriers at the CCSD(T)/6-311++G(2d,2p)//B3LYP/6-311++G(d,p) level, including zero-point energy corrections, turned out to be 6.21 kcal/mol, 3.88 kcal/mol and 3.55 kcal/mol, respectively. These results indicate that the addition-elimination channel is not significant at room temperature and below, although it might contribute a few percent at temperatures well above room temperature.

At this point it is evident that opposite results exist about the weight of the addition-elimination pathway in the overall acetone + OH reaction. As a consequence, the cause of the negative temperature dependence observed by Crowley and coworkers[3] below 240 K is not clear at all. Then, in this paper we intend to carry out the first variational transition-state theory rate constant calculations including multidimensional tunneling corrections of the different channels of the acetone + OH reaction, with the aim of shedding light on its controversial kinetics.

2. Method of Calculation

In this section we will successively describe the technical details for the electronic structure and the dynamical calculations.

Electronic Structure Calculations. Geometry optimization, energies, first and second energy derivatives for the title reaction were calculated at the B3LYP/6-31G(d) level of theory.[9] Energies at all the stationary points were then recalculated at a higher level of theory, the CBS-RAD multilevel energy method.[10] The CBS family of methods involves two basic elements: an extrapolation to an infinite basis set and an additive correction to the electron correlation treatment. Particularly, the procedure based on B3LYP/6-31G(d) geometries and zero-point energy corrections (ZPE) that we used is called CBS-RAD(B,B),[10] and it has been proved to give good enthalpies of formation for open-shell molecules with low spin contamination (i.e., $(<S^2>)<1.2$ for doublets), which is the case of the present system. The CBS-RAD(B,B) method obtains the energy from three single-point energy calculations at the B3LYP/6-31G(d) optimized geometries:

a) CCSD(T)(fc)/6-31+G†,

b) MP4(SDQ)(fc)/6-31+G(d(f),d,p), also denoted MP4(SDQ)(fc)/CBSB4, and

c) MP2(fc)/6-311++G(3d2f,2df,2p), also denoted MP2(fc)/CBSB3, with the Gaussian keyword CBSextrap=(nmin=10,pop).

For open-shell species, unrestricted open-shell reference wavefunctions are employed in steps (a)-(c). Notice that all these energy calculations treat the electron correlation within the frozen core approximation. For simplicity we will omit the (fc) notation from now on, and only the full correlation treatment will be explicitly detailed when used. The values obtained in steps (a)-(c)

are combined to obtain the multilevel CBS-RAD energy.[10-11] It has to be noted that the CBS-RAD(B,B) scheme includes the B3LYP/6-31G(d) ZPE scaled by 0.9806. In this paper the CBS-RAD(B,B) calculations without the ZPE correction will be denoted CBS-RAD (classical).

At this point, some results that will be discussed in the next section have to be introduced in order to understand the methodology we have employed. Several stationary points were found in the B3LYP/6-31G(d) PES, which correspond to three different reaction pathways (see Fig. 1 and 2): two for H-abstraction of acetone, and another for the addition of the hydroxyl radical to the carbon atom of the carbonyl group, followed by the elimination of a methyl group. The differences between the two H-abstractions arise from the position of the abstracted H atom: it can be eclipsed or alternated to the carbonyl group. The reaction products are the same for both abstractions. Each mechanism was found to proceed via a complex in the entrance channel (we will comment later on these complexes) and a saddle point structure. Also for the H-abstraction reactions a complex was found at the product side of the reaction, the same structure for both abstraction pathways. Although with substantial differences in the relative energies, the same reaction profiles were found at the CBS-RAD (classical) level of theory. Before going further, it will be useful to establish a nomenclature for each mechanism. Thus we will use the following notation (see together with Fig. 1 and 2):

Eclipsed. The pathway for the abstraction of a hydrogen atom eclipsed to the carbonyl group, that is, the reaction from R to P_1, going via CR_{ec}, SP_{ec} and CP_1. Within this mechanism several regions are also distinguished: *eclipsed association,* from R to CR_{ec}; *eclipsed abstraction,* from CR_{ec} to CP_1, through SP_{ec}; *dissociation*, from CP_1 to P_1.

Alternated. The pathway for the abstraction of a hydrogen atom in an alternated position to the carbonyl group, that is, the reaction from R to P_1, going via CR_{al}, SP_{al} and CP_1. The regions for this mechanism are: *alternated association,* from R to CR_{al}; *alternated abstraction,* from CR_{al} to CP_1, through SP_{al}; *dissociation*, from CP_1 to P_1. Note that the later region is the same for both hydrogen-abstraction pathways.

Addition-Elimination. The mechanism for the addition of the OH molecule to the carbon atom of the carbonyl group, followed by the elimination of a methyl group. That is, the reaction from R to P_2, going via CR_{add}, SP_{add}, P_{add} and SP_{el}. Three regions will be distinguished: *addition association,* from R to CR_{add}; *addition,* from CR_{add} to P_{add}, through SP_{add}; *elimination*, from P_{add} to P_2, via SP_{el}.

To ensure the connectivity between the stationary points found and for the dynamical calculations, the minimum energy path (MEP)[12] in an isoinertial mass-weighted Cartesian coordinate system was calculated starting from each saddle-point geometry found, that is, SP_{ec},

SP_{al}, SP_{add} and SP_{el} (see Fig. 1), by following the Page-McIver algorithm[13] at the B3LYP/6-31G(d) level of theory. A step size, $\boldsymbol{ds}$, of 0.02 bohr (where s denotes the distance along the MEP in an isoinertial mass-scaled coordinate system with a scaling mass equal to 1 amu) was used in all cases. The second derivative matrix was calculated at every two points of each MEP. For the eclipsed abstraction, a total of 365 non-stationary points along the MEP were calculated, from s=-3.90 to s=+3.40 bohr (s=0 at the saddle point, negative on the reactant side of the saddle point and positive on the product side); for the alternated abstraction, 342 points from s=-3.44 to +3.40 bohr; in the addition region, 322 points from s=-4.92 to +1.52 bohr; and for the elimination, 200 points from s=-2.00 to +2.00 bohr. For these four regions, the interpolated single-point energy correction (ISPE)[14] procedure was used for the variational transition-state calculations. The ISPE method is a dual-level direct dynamics scheme that uses a low-level (LL) MEP, and corrects the energy by interpolating the energy differences at some points along the MEP between this LL MEP and single-point energy calculations at a higher level (HL). In this work we used the B3LYP/6-31G(d) method as the LL and the CBS-RAD (classical) as the HL. Thus, in addition to the stationary points, we calculated the HL energy at several non-stationary points along the MEPs; for the eclipsed abstraction MEP at 10 non-stationary points with s values of -3.00, -1.00, -0.32, -0.24, -0.16, -0.12, -0.08, -0.04, +0.04 and +1.00 bohr; for the alternated abstraction at 11 points at s= -2.00, -1.00, -0.24, -0.16, -0.08, -0.04, +0.04, +0.08. +0.16, +0.24 and +1.00 bohr; in the addition region 9 points at s= -1.00, -0.32, -0.16, -0.08, +0.08, +0.16, +0.32, +0.80 and +1.00 bohr. Finally, for the elimination we used the HL energy at 5 non-stationary points with s= -1.00, -0.48, -0.12, +0.12 and +1.00 bohr. Due to the change of the electronic calculation level, in general, the HL classical energy maximum structure (with energy V_{max}) along the LL MEP will not coincide with the LL saddle point structure. The normal-mode analysis along the MEPs was performed in redundant internal coordinates, and the reoriented dividing surface (RODS)[15] algorithm was used to improve the obtained generalized frequencies.

For the eclipsed and alternated association regions we constructed a distinguished reaction coordinate path (DCP) at the B3LYP/6-31G(d) level, by fixing the internuclear distances $R(O_{11}-O_6)$ and $R(O_{11}-H_9)$, respectively (see Fig.1). In the eclipsed association the other degrees of freedom were allowed to relax. A total of six non-stationary points were used in the eclipsed association from $R(O_{11}-O_6)$=5.26Å to CR_{ec} (with $R(O_{11}-O_6)$=2.86Å). Since the MEP was not calculated for this region, the use of the RODS algorithm becomes necessary in order to obtain reliable generalized eigenvectors and frequencies along the DCP path. For the alternated association region, the calculation of the DCP presented some numerical problems and at some points it was not possible to optimize. The details for this association region will be explained in

the next section. Finally, the DCP was not calculated either for the dissociation or the addition association regions, as it will be also explained later. At each geometry of the eclipsed and alternated association DCPs, a generalized normal-mode analysis was done in rectilinear coordinates and the HL energy was computed.

Geometry optimization and the Hessian matrix calculation of the stationary points, the DCPs and all the single-point CBS-RAD (classical) multilevel energy calculations were carried out with the GAUSSIAN98 system of programs.[16] The GAUSSRATE8.7 code,[17] which is an interface linking POLYRATE8.7[18] and GAUSSIAN94,[19] was used for calculating the LL information along the MEPs.

Dynamical calculations. As we have already commented, we found that the reaction of acetone with the hydroxyl radical can proceed via three pathways. They are therefore three competitive reactions. To obtain the global reaction rate constant we applied the competitive canonical unified statistical (CCUS) theory,[20] in which the global reaction rate constant, $k^{CCUS}(T)$, is given by:

$$k^{CCUS}(T) = k^{EC}(T) + k^{AL}(T) + k^{ADD-EL}(T) \tag{1}$$

where $k^{EC}(T)$, $k^{AL}(T)$ and $k^{ADD-EL}(T)$ are the rate constants for the eclipsed, alternated and addition-elimination mechanisms, respectively. As several complexes are formed along these three mechanisms, there can be several bottlenecks in each pathway. Actually, there could be one at every of the above described regions. In this situation, the canonical unified statistical (CUS)[21] theory has to be applied, and the rate constants will be given by:

$$\frac{1}{k^{EC}(T)} = \frac{1}{k_{as,ec}(T)} - \frac{1}{k_{CR_{ec}}(T)} + \frac{1}{k_{ab,ec}(T)} - \frac{1}{k_{CP_l}(T)} + \frac{1}{k_{di}(T)} \tag{2.1}$$

$$\frac{1}{k^{AL}(T)} = \frac{1}{k_{as,al}(T)} - \frac{1}{k_{CR_{al}}(T)} + \frac{1}{k_{ab,al}(T)} - \frac{1}{k_{CP_l}(T)} + \frac{1}{k_{di}(T)} \tag{2.2}$$

$$\frac{1}{k^{ADD-EL}(T)} = \frac{1}{k_{as,add}(T)} - \frac{1}{k_{CR_{add}}(T)} + \frac{1}{k_{add}(T)} - \frac{1}{k_{P_{add}}(T)} + \frac{1}{k_{el}(T)} \tag{2.3}$$

$k_{CR_{ec}}(T)$, $k_{CR_{al}}(T)$, $k_{CR_{add}}(T)$, $k_{CP_l}(T)$ and $k_{P_{add}}(T)$

7

where are the one-way flux rate constants evaluated at the complexes formed along the reaction paths. The $k_{as,ec}(T)$, $k_{ab,ec}(T)$, $k_{di}(T)$, $k_{as,al}(T)$, $k_{ab,al}(T)$, $k_{as,add}(T)$, $k_{add}(T)$, and $k_{el}(T)$ are the rate constants for the eclipsed association, eclipsed abstraction, dissociation of CP_1, alternated association, alternated abstraction, addition association, addition and elimination regions, respectively. All these rate constants, except $k_{di}(T)$, were calculated by means of canonical variational transition-state $(CVT)^{22-26}$ theory, corrected with the multidimensional small-curvature tunneling $(SCT)^{27-30}$ coefficient when quantum effects on the nuclear motion were possible. That is, when the reaction has a positive adiabatic ground-state potential energy, $V_a^G(s)$, somewhere along the reaction path. The adiabatic potential energy includes classical potential energy and zero point energy contributions. The $k_{di}(T)$ rate constant was not calculated as it is not expected to have any dynamical effect on the global rate constant due to the high exothermicity of the abstraction reactions. The CVT/SCT rate constant is defined as:

$$k^{CVT/SCT}(T, s_*) = \mathbf{\kappa}^{SCT}(T)\mathbf{\sigma} \frac{k_B T}{h} \frac{Q^{GT}(T, s_*)}{Q^R(T)} \exp\left(- V(s_*)/k_B T\right) \tag{3}$$

where $\kappa^{SCT}(T)$ is the SCT transmission coefficient, s_* is the value of s at the free energy maximum along the reaction path (MEP or DCP) at temperature T, σ is the symmetry factor, k_B is Boltzmann's constant, h is Planck's constant, $V(s_*)$ is the classical potential energy at s_* with zero of energy at the overall classical energy of reactants, $Q^R(T)$ is the reactant partition function per unit volume again with zero of energy at reactants, and $Q^{GT}(T,s_*)$ is the generalized transition-state partition function with zero of energy at $V(s_*)$ and excluding the reaction coordinate. For all the partition functions the rotational symmetry numbers are removed, as they are included in σ. Note that, in spite of the separation in different regions that we have done for each mechanism, according to the CUS theory all the rate constants are calculated with the same reactants, acetone and OH. Therefore $Q^R(T)$ is the same in all cases. The addition-elimination mechanism rate constant was calculated with the CUS theory, in which the product formed by the addition (P_{add}) was treated as a minimum along the path but not as a stabilized intermediate. The rapid elimination of the methyl group of the rovibrationally excited P_{add} formed in the addition of OH to acetone, makes the addition-elimination reaction go ahead without stabilization of P_{add}.[7]

As we have already mentioned, for the regions with a saddle point we used the ISPE algorithm. This method is based on a mapping function[31] to interpolate the information along the MEP. For the association regions a three-point Lagrange interpolation was used. In all cases the vibrational partition functions were evaluated within the harmonic approximation.

The calculations of $k_{add}(T)$ and $k_{el}(T)$ were made with the GAUSSRATE8.7[17] interface, while for the other rate constant calculations the POLYRATE8.7[18] code was used.

3. Results and discussion.

In this section the results for the three pathways will be first presented separately. Afterward, the evaluation of the contribution of each one to the global mechanism and rate constant will be discussed.

Although the density functional theory (DFT) methods have provided a poor description for the barrier heights of this kind of hydrogen-abstraction reactions,[32-38] geometries and frequencies are generally in reasonable agreement with other *ab initio* electronic levels such as MP2, QCISD(T) or CCSD(T). Therefore, the use of B3LYP/6-31G(d) geometries, gradients and frequencies for the calculation of the CBS-RAD(B,B) energy profiles, does not necessarily suffer from the expected bad energetics given by the DFT methods. In addition, if our purpose is to calculate rate constants the main feature we need from an electronic method is an accurate description of the energy profile (classical potential energy, zero-point energy corrections and free energy profiles). By now, it seems that this cannot be accomplished by any computationally affordable single-level electronic method and one has to use a dual-level approach (geometry optimization at a low level and single-point energy calculation at a higher level). One possibility is to make the calculation of the high-level energy in one of the so-called multilevel energy schemes,[39-46] some of which seem to provide rather balanced potential energy surfaces. This could be the case of the CBS-RAD(Q,Q)[10] multilevel method (where (Q,Q) stands for QCISD(fc)/6-31G(d)[47] geometries and vibrational frequencies), not only for the hydrogen-abstraction reaction but also for the addition-elimination pathway. However, the QCISD(fc)/6-31G(d) vibrational frequency calculations along the MEP could be too time consuming. Therefore, we have chosen the CBS-RAD(B,B) scheme which, as mentioned, is expected to give reasonable energies for the present open-shell system.

The dynamical calculations were carried out at both the B3LYP/6-31G(d) and the CBS-RAD(B,B) levels but, according to what we have explained about the B3LYP energies, only the CBS-RAD(B,B) rate constants will be detailed. However, at the end of this section the B3LYP dynamical results will be introduced in the discussion of the results.

A. Eclipsed pathway results.

In Table 1 the energetics for all the regions that we have identified in the acetone + OH reaction are given at the two levels of theory used in our calculations.

As it has already been found by other authors, the abstraction of a hydrogen atom eclipsed to the carbonyl group takes place via the formation of a complex in the entrance channel (CR$_{ec}$ depicted in Fig.1). Its relatively high stabilization (-9.70 kcal/mol and –6.82 kcal/mol, for the classical potential B3LYP/6-31G(d) and the CBS-RAD (classical) energies, respectively) is mainly due to the interaction between the hydrogen atom of the hydroxyl radical and the oxygen atom of the carbonyl group in acetone. The DCP constructed for this association region does not present any saddle point nor a maximum of the adiabatic energy. Only when the free energy is evaluated along the DCP a maximum appears, so that the variational transition-state rate constant can be calculated for this eclipsed association. The $k_{as,ec}(T)$ values obtained at the CBS-RAD(B,B) level with a symmetry number (σ) equal to 2, are given in Table 2. Note that, as there is not any saddle point, the conventional transition-state rate constant (k^{TST}) cannot be evaluated and that, with the lack of an adiabatic barrier, tunneling definition has no sense. As it can be seen, the $k_{as,ec}(T)$ values show a negative temperature dependence.

In the product side of the eclipsed pathway we found another complex, CP$_1$ (see Fig.1), with a classical potential energy of –24.95 and –29.25 kcal/mol at the B3LYP/6-31G(d) and the CBS-RAD (classical) levels, respectively (see eclipsed abstraction rows in Table 1). Presumably, it is the same as the one found by Peeters and coworkers[7] for what they call the indirect abstraction (corresponding to the eclipsed mechanism in the present paper). Due to the large exothermicity of the abstraction we assumed that this dissociation will take place without any contribution to the overall eclipsed abstraction rate constant. Therefore, we did not calculate the DCP for this dissociation region.

If we assume that the reaction enthalpy will be close to the adiabatic energy of reaction, we can compare our values in Table 1 (see Dissociation region) to the reaction enthalpy of –21.03 kcal/mol evaluated by Crowley and coworkers[3] from experimental enthalpies of formation.[48-51] The B3LYP/6-31G(d) result underestimates the exothermicity by 5.10 kcal/mol, whereas at the CBS-RAD(B,B) level it is overestimated by 1.98 kcal/mol. For the saddle point of the eclipsed abstraction large differences are also observed between the two electronic methods. As expected, the B3LYP classical energy barrier (V) is lower than the CBS-RAD (classical) one (V_{max}). When the zero-point energy (ZPE) correction is added, the resulting B3LYP adiabatic energy at the saddle point lies –0.52 kcal/mol below the zero-point energy of reactants, but the maximum of the adiabatic energy profile (V^{AG}) is located at s=-0.24 bohr and has a value of 0.29 kcal/mol. At the CBS-RAD (classical) level, the classical potential energy evaluated at the B3LYP saddle point (s=0 bohr) is 2.02 kcal/mol, but its maximum (V_{max}) is 0.58 kcal/mol higher and occurs at s=-0.13 bohr. The CBS-RAD(B,B) adiabatic energy barrier is 2.86 kcal/mol, that is,

0.94 kcal/mol higher than the adiabatic energy at V_{max}. These values indicate that variational effects can be important. This can be seen in the resulting CBS-RAD(B,B) rate constants for the eclipsed abstraction region presented in Table 2, calculated with $\sigma=4$. Variational effects make the rate constants (k^{CVT}(T)) one order of magnitude and 2.5 times slower than the corresponding TST ones at 202 and 1500 K, respectively. The tunneling correction (κ^{SCT}) goes in the opposite way, with a value of 22 at 202 K and 1.06 at 1500 K.

The one-way flux rate constant evaluated at the eclipsed association complex, $k_{as,ec}$(T), is expected to be much higher than the ones calculated for the other regions of the eclipsed mechanism. As a consequence, it would not have any effect on the overall eclipsed rate constant and we have not calculated it.

The calculation of the overall eclipsed rate constant, k^{EC}(T) (see Table 5), by Equation 2.1 (with the commented modifications), shows that there is no contribution from the association region at any of the temperatures studied. This is because the association rate constant is very much faster than the eclipsed abstraction one up to 700 K. At temperatures above 700 K the eclipsed association free energy maximum collapses to the eclipsed abstraction free energy profile, and the eclipsed pathway proceeds via a unique dynamical bottleneck. Consequently, the canonical unified statistical theory is not applied anymore and the overall eclipsed rate constant is again the one corresponding to the abstraction process itself.

B. Alternated pathway results.

Although Dóbé, Henon and coworkers[6] did not find what we have called the alternated saddle point, and Peeters and coworkers[7] found it but they considered this pathway as a direct abstraction, our results show that the general scheme for this mechanism is similar to the eclipsed one. The products obtained and the complex formed in the product side are the same as for the eclipsed reaction (see Fig.1 and 2). However, the detailed mechanism is significantly different. The saddle point structure found for the alternated abstraction has a classical potential energy of 0.40 kcal/mol at the B3LYP/6-31G(d) level (Table 1). At the CBS-RAD (classical) level, the energy for this structure is 2.23 kcal/mol higher, and the maximum of the classical potential energy profile (V_{max}) occurs at s=-0.14 bohr, giving a barrier height of 2.98 kcal/mol. Again the B3LYP classical potential energy barrier is lower than the CBS-RAD (classical) value. Moreover, the relative classical energies of the two abstraction pathways have inverted their positions. At the CBS-RAD (classical) level, the eclipsed maximum is 0.38 kcal/mol more stable than the alternated one (it is not a large difference but the barrier heights are also small). It seems reasonable because, as can be seen in Fig. 1, the SP_{ec} structure still keeps part of the stabilizing

hydroxyl radical interaction with the carbonyl group found in CR_{ec}. The adiabatic barrier height (V^{AG}) is 2.85 kcal/mol (curiously almost the same value as for the eclipsed abstraction), which is 0.52 kcal/mol higher than the CBS-RAD(B,B) adiabatic energy at the CBS-RAD (classical) potential energy maximum ($V_a^G(V_{max})$). Note that the addition of the ZPE correction makes the alternated abstraction barrier slightly lower, whereas for the eclipsed abstraction it is increased by 0.26 kcal/mol. We will return to that point later. The CBS-RAD(B,B) rate constants for the alternated abstraction region, $k_{ab,ec}(T)$, are presented in Table 3. The symmetry number corresponding to this region is 4. The variational effects are smaller than in the eclipsed abstraction. They slow down the rate constants by a factor of 2.4 and 1.03 at 202 and 1500 K, respectively. Also the tunneling correction is less important, with a value of 4.4 at 202 K. Since the adiabatic barrier heights are practically the same for both pathways, the larger tunneling correction for the eclipsed abstraction correlates with the narrower adiabatic energy profile provoked by the more stable complex in the entrance channel.

Initially we could not find the association complex for the alternated pathway, CR_{al}, on the B3LYP/6-31G(d) PES, probably due to the proximity of the CR_{ec} well. However, when calculating the MEP towards reactants for the H-abstraction at the B3LYP/6-31G(d) level, we found a point with a converged gradient, which lies 2.46 kcal/mol below reactants (see Fig. 1 and Table 1). It has a $R(O_{11}-H_9)$ distance of 2.08 Å and it is located at s=-3.44 bohr. When the CBS-RAD (classical) energy was evaluated along the B3LYP reaction path, it also presented a minimum but at a B3LYP structure with $R(O_{11}-H_9)$=2.05 Å. The CBS-RAD reaction energies for the alternated association given in Table 1 correspond to this structure. The B3LYP well is 0.77 kcal/mol deeper than the CBS-RAD (classical) one, whose CBS-RAD(B,B) adiabatic energy is -0.88 kcal/mol. Thus, an association region can also be defined for the alternated reaction in terms of both classical and adiabatic potential energy. As there is not a saddle point for the formation of this complex, and in order to calculate the CVT CBS-RAD(B,B) rate constants, we constructed a B3LYP/6-31G(d) DCP starting at the structure with $R(O_{11}-H_9)$=2.05 Å. This region of the potential energy surface is very smooth which, together with the proximity of the quite deep CR_{ec} complex, make the optimization and the calculation of second derivatives quite difficult. Because of that, only four points along this DCP could be calculated. However, the evaluation of the free energy profile for this association region between 150-1500K, shows that the minimum disappears, and no maximum is found. Therefore, although the existence of CR_{al} in terms of adiabatic energy contributes to the rate constant obtained for the alternated abstraction region (it enhances tunneling), there is not a dynamical bottleneck for the alternated association region, and the rate constant for the overall alternated mechanism is the one corresponding to the abstraction

itself. Looking at the CR_{al} and SP_{al} structures depicted in Fig. 1, it can be seen that they are nearly the same but with a different value for the $R(O_{11}-H_9)$ distance. Thus, from the reactants separated at an infinite distance to SP_{al}, the reaction path involves basically one motion, the decrease of $R(O_{11}-H_9)$.

C. Addition-Elimination pathway results.

This is the mechanism that Crowley and coworkers[3,4] proposed as a potentially responsible for the observed increase of the acetone + OH rate constants at low temperatures. The final products are acetic acid and the methyl radical (P_2 in Fig.1 and 2), and it proceeds via the addition of the hydroxyl radical to the carbon of the carbonyl group in acetone. The classical potential reaction energy for the overall pathway is –25.68 and –29.25 kcal/mol at the B3LYP and CBS-RAD (classical) levels, respectively (see the elimination rows in Table 1). When ZPE corrections are added, the B3LYP adiabatic energy of reaction is 0.37 kcal/mol underestimated, when compared to the value of –26.03 kcal/mol given by Crowley and coworkers[3,48-51] for the exothermicity. In contrast, at the CBS-RAD(B,B) level the exothermicity is again overestimated (by 3.2 kcal/mol). For the addition region, the CBS-RAD (classical) potential energy (-20.38 kcal/mol) differs by 1.15 kcal/mol from the B3LYP result. Note that the classical and adiabatic reaction energies given in Table 1 for this region correspond to the formation of P_{add}. The inclusion of ZPE corrections increases its energy, as expected according to the formation of the new C-O bond.

We found a saddle point in both the addition and the elimination regions. For the addition region, the B3LYP classical potential energy of SP_{add} is negative, and at the CBS-RAD (classical) level the energy barrier height is only 0.94 kcal/mol. From these results one could erroneously conclude, comparing to the abstraction energy barriers, that the addition mechanism will be faster than the abstraction ones. However, after correction for the zero-point energies the addition adiabatic barrier (V^{AG}) at the CBS-RAD(B.B) level becomes 0.5 kcal/mol higher than the abstraction ones. Moreover, the differences between the free energy barriers corresponding to the addition and the abstraction pathways must be larger as it can be derived from the slow rate constants obtained for the addition region at the CBS-RAD(B,B) electronic level (see Table 4). For this region, we have taken $\sigma=4$. Further discussions comparing the three mechanisms will be done in part D. The variational effects for this addition region are small at low temperatures ($k^{CVT}/k^{TST} = 0.94$ at 202 K) and slightly increase with temperature (at 1500 K they slow down the rate constant leading to $k^{CVT}/k^{TST} = 0.82$). The effective tunneling potential barrier (V^{AG}) is higher than the abstraction reaction ones, the tunneling correction being only 1.54 at 202 K. The

well (CR$_{add}$) in the entrance channel is quite deep, so it favors tunneling. However, the ZPE correction makes the adiabatic energy profile wider, especially in the product side of the addition region. This results in a small transmission coefficient (κ^{SCT}).

For the elimination of the methyl group, the calculated adiabatic energy barrier is –9.98 and –9.50 kcal/mol with respect to acetone + OH at the B3LYP and CBS-RAD(B,B) levels, respectively. The resulting rate constant taking acetone + OH as the reactants are very fast at low temperatures but decrease rapidly with increasing temperature (see Table 4). As a result, the evaluation of the overall k^{ADD-EL}(T) by Equation 2.3 shows a small contribution of the elimination rate constant at temperatures higher than 1000 K (Table 5). Note that at low temperatures, the rate constants for the overall addition-elimination mechanism do not increase with decreasing temperature.

The rate constants for the association region of this mechanism and the one-way flux rate constant at the addition association complex (k$_{as,add}$(T)) have not been calculated as they are expected to be very much faster than the addition ones at all temperatures considered.

D. Overall acetone + OH rate constant

Once we have calculated the rate constants for each of the three possible pathways identified for the acetone + OH reaction, they are combined as competitive mechanisms following Equation 1 (see Table 5 for the CBS-RAD(B,B) results). These values show that, for the whole range of temperatures, the addition-elimination rate constants are one, two or even more orders of magnitude lower than the abstraction rate constants. Consequently, not only the addition-elimination mechanism does not become faster with decreasing temperature, but also its contribution to the global rate constant is very small: k^{CCUS}(T) is basically the sum of the two abstraction rate constants. Actually, our CBS-RAD(B,B) adiabatic barrier height (V^{AG} in Table 1) for the addition region is 4.82 and 2.92 kcal/mol lower than the values reported by Dóbé and coworkers[6] and Peeters and coworkers,[7] respectively. Then our CBS-RAD(B,B) rate constant for the addition region at 298 K is 316 times higher than the calculated value by Peeters and coworkers.[7] However, the CBS-RAD(B,B) k^{ADD}(T), and thus k^{ADD-EL}(T), are still very low. Moreover, at the B3LYP/6-31G(d) level, with an adiabatic barrier height of only 1.87 kcal/mol, the addition-elimination rate constant does not increase with decreasing temperature, and lies between 5.2×10^{-16} and 9.5×10^{-14} cm^{3}molecule^{-1}s^{-1} in the temperature range studied in this work. Hence, our calculations agree with the conclusions of Dóbé, Henon and coworkers[6] and Peeters and coworkers[7] that the addition-elimination mechanism cannot be the responsible for the negative temperature dependence observed at low temperatures for the acetone + OH reaction.

Note that in the case that the addition association, not calculated in this work, was slow enough to contribute to the overall addition-elimination rate constant, its contribution would make $k^{ADD-EL}(T)$ even lower (see Equation 2.3).

At both the CBS-RAD(B,B) and the B3LYP levels, our results are that $k^{CCUS}(T)$ is basically the sum of the two abstraction rate constants. It can be seen in Table 5, that at the CBS-RAD(B,B) level, the alternated pathway clearly dominates at high temperatures. When temperature decreases the eclipsed rate constant equals the alternated value, and below 210 K it becomes the faster mechanism. This results in that the eclipsed Arrhenius plot is more curved than the alternated one (see Fig. 3). However, the two mechanisms have the same adiabatic energy barrier (V^{AG} in Table 1). At low temperatures we have already explained the differences in terms of tunneling corrections. At higher temperatures, the slowdown of $k^{EC}(T)$ could be due to a large negative entropic barrier. For the eclipsed mechanism the ZPE corrections, as mentioned, increase the barrier height as a consequence of the interaction $>C=O\text{---}H\text{--}O$. A tight transition state would then imply an entropic restriction to the reaction rate. To quantify these differences between the two abstractions, we have decomposed the free energy barriers at 202 and 1000 K into their enthalpic and entropic contributions (see Table 6). We have also distinguished between these quasi-thermodynamic activation magnitudes evaluated at the free energy maximum ($\Delta H^{GT}(T,s_*)$, $\Delta S^{GT}(T,s_*)$), that is at the temperature-dependent variational or generalized transition state, and their contribution due to tunneling ($\Delta H^{TUN}(T)$, $\Delta S^{TUN}(T)$).[53,54] The values $\Delta H^{TOT}(T,s_*)$ and $\Delta S^{TOT}(T,s_*)$ given in Table 6 are the total quasi-thermodynamic magnitudes, that is for example, $\Delta H^{TOT}(T) = \Delta H^{GT}(T,s_*) + \Delta H^{TUN}(T)$. The same analysis was done for the addition region.

At 1000 K, the eclipsed and the addition pathways have similar generalized enthalpic barriers, $\Delta H^{GT}(1000\ K,s_*) = 1.89$ and 1.74 kcal/mol, and the alternated barrier is the highest (2.33 kcal/mol). However, the generalized entropic barrier for the eclipsed and, even more, for the addition regions are clearly more negative than for the alternated one (-23.46, -26.67 and -18.63 cal/mol K, respectively). The high temperature makes the generalized entropic effect dominate and the consequence is that $k^{ADD} < k^{EC} < k^{AL}$, as it can be seen in Tables 2, 3 and 4 for the $k^{CVT}(T)$ values. At high temperatures, tunneling contribution is not very important and the relative order of the three mechanisms stays the same. Thus, the eclipsed and the addition rates at high temperatures will be restricted by the entropic effect.

Conversely, at 202 K the mechanisms that have the same generalized enthalpic barrier are the alternated and the addition, $\Delta H^{GT}(202\ K,s_*)=1.98$ kcal/mol, and the eclipsed one is 0.26 kcal/mol lower. However, the larger generalized entropic barriers for the eclipsed and addition

pathways (-26.04 and –28.71cal/molK) still make the alternated abstraction the faster reaction (see k^{CVT}(202 K) in Tables 3, 4 and 5). Note that because of the lower temperature, the differences in k^{CVT}(202 K) due to the entropic effect are smaller than at 1000 K. When tunneling is included, the total enthalpic barrier height for the eclipsed mechanism is drastically reduced. Actually it becomes negative (-0.44 kcal/mol). This explains that at low temperatures the eclipsed mechanism turns out to be the fastest. For the addition pathway the tunneling contribution is relatively small, so that the rate constants remain small compared to the abstraction ones.

With the values obtained for the CBS-RAD(B,B) rate constants, we have calculated the branching ratio for the addition-elimination mechanism, k^{ADD-EL}(T)/k^{CCUS}(T), given in Table 7. At all range of temperatures, the addition-elimination mechanisms accounts only for the 0.12-2.05 % of the acetone + OH reaction. These values agree with the upper limit of 3% given by Peeters and coworkers,[7] and not with the branching ratio of 50% measured by Wollenhaupt and Crowley.[4] As it can be seen k^{ADD-EL}(T)/k^{CCUS}(T) increases from 150 to 700 K, has a maximum between 700 and 800 K, and then it slightly decreases. This is probably as a result of the balance between tunneling and entropic barrier height: at low temperatures the abstraction reactions are very much faster due to tunneling, increasing temperature decreases tunneling correction, and at high temperatures, the high entropic barrier for the addition pathway accentuates again the difference between the abstraction and the addition rate constants. At the B3LYP/6-31G(d) level, the branching ratio for the addition-elimination mechanism is even smaller (0.04-1.06%, from 150 to 1500 K), and it increases in the range 150-1200 K and above that remains constant.

The comparison between our results for the overall rate constants and the experimental results (see Table 5) shows that the CBS-RAD(B,B) rate constants somewhat underestimate the experimental ones. At 1217 K, the experimental value is 4.9 times the calculated one. At lower temperatures the differences become larger, with a ratio of 17.8 (k_{exp}/k_{calc}) at 202 K. There are mainly two reasons that could explain the lower calculated results: it may be another competitive mechanism missing in our calculations, or the CBS-RAD(B,B) barrier heights (in terms of free energy) are somewhat too high. In addition, although the CBS-RAD(B,B) rate constants result in a curved Arrhenius plot (solid line in Figure 3), they do not show a negative temperature dependence at low temperatures.

Peeters and coworkers[7] pointed out in their work, although they did not do the calculation, that a low-lying transition state for the H-abstraction pathway via the hydrogen-bonded complex (the eclipsed mechanism in this work) could lead to the experimentally observed Arrhenius plot. It is true that with appropriate relative energies two consecutive bottlenecks (as the eclipsed association and abstraction ones) could lead to the observed Arrhenius behavior for the acetone +

OH reaction. Actually the eclipsed association region is the only region that presents a negative temperature dependence in our calculations at the CBS-RAD(B,B) level. Despite this, $k_{as,ec}(T)$ is too high to significantly contribute to the overall rate constant (specially at low temperatures where it will be required to be important). As we have seen in Table 2, at low temperatures it is $\sim 10^{-10}$ cm^{3}molecule^{-1}s^{-1}. Thus, when this order of magnitude is compared to the eclipsed abstraction value ($\sim 10^{-15}$ cm^{3}molecule^{-1}s^{-1} at low temperatures), and also to the experimental value for the overall reaction ($\sim 10^{-13}$ cm^{3}molecule^{-1}s^{-1}), the conclusion is that the association occurs too rapidly to make the overall rate constants increase at low temperatures. Then, we think that the eclipsed association cannot be the origin of the negative activation energies observed at low temperatures.

A final consideration will be done in this Results and Discussion section. In Figure 3 we have seen that the Arrhenius plot at the CBS-RAD(B,B) level for the overall reaction, and even more for the eclipsed mechanism, is very curved. The experimental plot by Crowley and coworkers[3] not only is very curved but also seems to have a slightly negative activation energy at low temperatures. However, our results do not show this negative temperature dependence. As a matter of fact, very recent experimental results by Ravishankara and coworkers[55] show an essentially constant rate at and below about 250 K. Moreover, our overall rate constants somewhat underestimate the experimental ones which could be, as mentioned, due to an overestimation of the abstraction barrier heights. Although we have already mentioned the problems that the DFT methods present in calculating barrier heights for this kind of hydrogen-abstraction reactions, we display the B3LYP/6-31G(d) Arrhenius plots in Figure 4, as an example of what could happen with lower abstraction transition states. As it can be seen, the three plots depicted (overall acetone + OH reaction, eclipsed and alternated pathways) have a positive activation energy at high temperatures, which turn out to be negative at low temperatures. As it has been observed for other reactions, this kind of Arrhenius plot can be a consequence of low, inexistent or even negative energy barriers. Effectively, at the B3LYP level the abstraction pathways have a small classical barrier height ($V(s=0)$ in Table 1), an even smaller adiabatic energy barrier (V^{AG}), both positive, and a negative generalized activation enthalpy. Thus, it would be possible that the Arrhenius behavior observed by Crowley and coworkers[3] for the acetone + OH reaction could be explained just with the abstraction mechanisms. We just would need an electronic method with the appropriate energy profiles. At the CBS-RAD(B,B) level, we have seen that the eclipsed mechanism, which leads to a very curved Arrhenius plot, has a negative total activation enthalpy at 202 K (see Table 6). However, its value of –0.44 kcal/mol is not negative enough to reproduce the observed negative activation energy. An accurate treatment

of a competitive mechanism, which is based on reactions with such small barrier heights but also with tunneling and variational contributions, is probably still a challenge for computational chemists.

4. Conclusions

In this paper we have performed the first variational transition-state theory rate constant calculations with multidimensional tunneling corrections of the acetone plus hydroxyl radical reaction. The interpolated single-point energy correction procedure was used for the variational calculations. In particular the B3LYP/6-31G(d) and the CBS-RAD multilevel energy methods have been employed as low-level and higher level, respectively. We have shown that three different reaction pathways exist:

a) Abstraction of a hydrogen atom eclipsed to the carbonyl group, which takes place through the formation of a hydrogen-bonded complex in the entrance channel, followed by the abstraction itself and another complex in the exit channel. The abstraction process entirely determines the value of the overall eclipsed rate constant, which have both important variational and tunneling contributions.

b) Abstraction of a hydrogen atom in an alternated position to the carbonyl group. In terms of both classical and adiabatic potential energy a complex appears before the saddle point of the abstraction itself and another after it. However, entropic effects suppress the entrance complex in terms of free energy between 150 and 1500 K, in such a way that the hydrogen abstraction takes place directly. Both the variational and the tunneling effects are smaller than for the eclipsed case.

c) OH-addition to the carbonyl C atom followed by methyl elimination, with a complex that appears before the addition saddle point. The overall rate constant for this pathway is entirely due to the OH-addition which has no significant tunneling. The corresponding Arrhenius plot exhibits a clear positive activation energy over all the temperature range, with only a slight curvature. On the other hand, comparing with the two abstraction rates, it can be seen that the rate constant of this addition-elimination mechanism has an almost negligible contribution to the global rate constant of the acetone + OH reaction at whatever temperature. The corresponding branching ratio turns out to be of at most ≈2%, thus confirming the experimental findings of Peeters and coworkers.[7] Interestingly, this branching ratio reaches its smaller values at low temperatures. For all those reasons, we conclude that the addition-elimination pathway cannot be the source of the experimental negative temperature dependence at low temperatures found by Crowley and coworkers.[3]

The global rate constant of the acetone + OH reaction turns out to be essentially the sum of the eclipsed and the alternated abstraction rate constants. The alternated abstraction is faster than the eclipsed one above 210 K. Below this temperature, the greater contribution of tunneling makes it possible that the eclipsed abstraction dominates. Comparing with the experimental results, our theoretical global rate constants are good enough, although they turn out to be somewhat underestimated, specially at low temperatures. They give a clearly curved Arrhenius plot, but no negative temperature dependence is obtained at low temperatures. At this respect, it would be interesting to guess how the potential energy surface of the acetone + OH system should be altered to reproduce the shape of the experimental Arrhenius plot found by Crowley and coworkers.[3] Unexpectedly our B3LYP/6-31G(d) low level results provides us a hint. An abstraction pathway with an adiabatic energy barrier for the abstraction process itself still positive, but small enough to produce a sufficiently negative generalized enthalpic barrier (just the case corresponding to the B3LYP/6-31G(d) low level results) would produce the adequate Arrhenius plot. Additional experimental and theoretical work would be necessary in order to clarify the reliability of that kinetic behaviour as a function of the temperature for the acetone + OH chemical system.

ACKNOWLEDGMENTS

References

[1] Wallington, T. J.; Kurylo M. J. *J. Phys. Chem.* **1987**, *91*, 5050.

[2] Le Calvé, S.; Hitier, D.; Le Bras, G.; Mellouki, A. *J. Phys. Chem. A* **1998**, *102*, 4579.

[3] Wollenhaupt, M.; Carl, S. A.; Horowitz, A.;Crowley, J. N. *J. Phys. Chem. A* **2000**, *104*, 2695.

[4] Wollenhaupt, M.; Crowley, J. N. *J. Phys. Chem. A* **2000**, *104*, 6429.

[5] Tranter, R. S.; Walker, R. W. *Phys. Chem. Chem. Phys.* **2001**, *3*, 1262.

[6] Vasvári, G.; Szilágyi, I.; Bencsura, Á.; Dóbé, S.; Bérces, T.; Henon, E.; Canneaux, S.; Bohr, F. *Phys. Chem. Chem. Phys.* **2001**, *3*, 551.

[7] Vandenberk, S.; Vereecken, L.; Peeters, J. *Phys. Chem. Chem. Phys.* **2002**, *4*, 461.

[8] Aloisio, S.; Francisco, J. S. *J. Phys. Chem. A* **2000**, *104*, 3211.

[9] Becke, A. M. *J. Chem. Phys.* **1993**, *98*, 5648.

[10] Mayer, P. M.; Parkinson, C. J.; Smith, D. M.; Radom, L. *J. Chem. Phys.* **1998**, *108*, 604.

[11] Ochterski, J. W.; Petersson, G. A.; Montgomery, Jr., J. A. *J. Chem. Phys.* **1996**, *104*, 2598.

[12] (a) Truhlar, D. G.; Kupperman, A. *J. Am. Chem. Soc.* **1971**, *93*, 1840; (b) Fukui, K. *Pure Appl. Chem.* **1982**, *54*, 1825.

[13] Page, M.; Mc Iver, J. W. *J. Chem. Phys.* **1988**, *88*, 922.

[14] Chuang, Y. -Y.; Corchado, J. C.; Truhlar, D. G. *J. Phys. Chem. A* **1999**, *103*, 1140.

[15] Villà, J.; Truhlar, D. G. Chem. Theor. Acc. **1997**, *97*, 317.

[16] (b) Frisch, M. J.; Trucks, G. W.; Schlegel, H. B.; Scuseria, G. E.; Robb, M. A.; Cheeseman, J. R.; Zakrzewski, V. G.; Montgomery, J. A.; Stratmann, R. E.; Burant, J. C.; Dapprich, S.; Millam, J. M.; Daniels, A. D.; Kudin, K. N.; Strain, M. C.; Farkas, O.; Tomasi, J.; Barone, V.; Cossi, M.; Cammi, R.; Mennucci, B.; Pomelli, C.; Adamo, C.; Clifford, S.; Ochterski, J.; Petersson, G. A.; Ayala, P. Y.; Cui, Q.; Morokuma, K.; Malick, D. K.; Rabuck, A. D.; Raghavachari, K.; Foresman, J. B.; Cioslowski, J.; Ortiz, J. V.; Stefanov, B. B.; Liu, G.; Liashenko, A.; Piskorz, P.; Kamaromi, I.; Gomperts, R.; Martin, R. L.; Fox, D. J.; Keith, T.; Al-Laham, M. A.; Peng, C. Y.; Nanayakkara, A.; Gonzalez, C.; Challacombe, M.; Gill, P. M. W.; Johnson, B. G.;Chen, W.; Wong, M. W.; Andres, J. L.; Head-Gordon, M.; Replogle, E. S.; Pople, J. A. *Gaussian 98*; Gaussian Inc.: Pittsburgh, PA, 1998.

[17] Corchado, J. C.; Chuang, Y. -Y.; Coitiño, E. L.; Truhlar, D. G. *Gaussrate 8.7*; University of Minnesota, 2001 (based on Polyrate 8.7[18] and Gaussian 94[19])

(http://comp.chem.umn.edu/polyrate)

[18] Corchado, J. C.; Chuang, Y. -Y.; Fast, P. L.; Villà, J.; Hu, W. -P.; Liu, Y. -P.; Lynch, G. C.; Nguyen, K. A.; Jackels, C. F.; Melissas, V.; Lynch, B. J.; Rossi, I.; Coitiño, E. L.; Fernández-Ramos, A.; Pu, J.; Steckler R.; Garrett, B. C.; Isaacson, A. D.; Truhlar, D. G. *Polyrate 8.7*; University of Minnesota, 2001 (http://comp.chem.umn.edu/polyrate).

[19] Frisch, M. J.; Trucks, G. W.; Schlegel, H. B.; Gill, P. M. W.; Johnson, B. G.; Robb, M. A.; Cheeseman, J. R.; Keith, T. A.; Petersson, G. A.; Montgomery, M. A.; Raghavachari, K.; Al-Laham, M. A.; Zakrzewski, V. G.; Ortiz, J. V.; Foresman, J. B.; Cioslowski, J.; Stefanov, B. B.; Nanayakkara, A.; Challacombe, M.; Peng, C. Y.; Ayala, P. Y.; Chen, W.; Wong, M. W.; Andres, J. L. ; Replogle, E. S.; Gomperts, R.; Martin, R. L.; Fox, D. J.; Binkley, J. S.; Defrees, D. J.; Baker, J.; Stewart, J. P.; Head-Gordon, M.; Gonzalez, C.; Pople, J. A. *Gaussian 94*; Gaussian Inc.: Pittsburgh, PA, 1995.

[20] Hu, W. -P.; Truhlar, D. G. *J. Am. Chem. Soc*. **1996***, 118*, 860.

[21] Hu, W. -P.; Truhlar, D. G. *J. Am. Chem. Soc*. **1995***, 117*, 10726.

[22] Garrett, B. C.; Truhlar, D. G. *J. Phys. Chem.* **1979**, *83*, 1079.

[23] Garrett, B. C.; Truhlar, D. G. *J. Chem. Phys.* **1979**, *70*, 1593.

[24] Garrett, B. C.; Truhlar, D. G.; Grev, R. S.; Magnuson, A. W. *J. Phys. Chem.* **1980**, *84*, 1730 ; Erratum: **1983**, *87*, 4554.

[25] Isaacson, A. D.; Truhlar, D. G. *J. Chem. Phys.* **1982**, *76*, 1380.

[26] Truhlar, D. G.; Isaacson, A. D.; Garrett, B. C. In *Theory of Chemical Reaction Dynamics*; Baer, M., Ed. ; (CRC Press: Boca Raton, FL, 1985; Vol. 4, pp. 65-137).

[27] Liu, Y. -P.; Lynch, G. C.; Truong, T. N.; Lu, D. -h.; Truhlar, D. G.; Garrett, B. C. *J. Am. Chem. Soc.* **1993,** *115*, 2408.

[28] Lu, D. -h.; Truong, T. N.; Melissas, V.; Lynch, G. C.; Liu, Y. -P.; Garrett, B. C.; Steckler, R.; Isaacson, A. D.; Rai, S. N.; Hancock, G. C.; Laurderdale, J. G.; Joseph, T.; Truhlar, D. G. *Comput. Phys. Commun.* **1992**, *71*, 235.

[29] Truhlar, D. G.; Gordon, M. S. *Science* **1990**, *249*, 491.

[30] Truong, T. N.; Lu, D. -h.; Lynch, G. C.; Liu, Y. -P.; Melissas, V.; Stewart, J. J. P.; Steckler, R.; Garrett, B. C.; Isaacson, A. D.; González-Lafont, A.; Rai, S. N.; Hancock, G. C.; Joseph, T.; Truhlar, D. G. *Comput. Phys. Commun.* **1993**, *75*, 143.

[31] Corchado, J. C.; Coitiño, E. L.; Chuang, Y. -Y.; Fast, P. L.; Truhlar, D. G. *J. Phys. Chem*. **1998**, *102*, 2424.

[32] Johnson, B. G.; Gonzales, C. A.; Gill, P. M. W.; Pople, J. A. *Chem. Phys. Lett*. **1994**, *221*, 100.

[33] Durant, J. L. *Chem. Phys. Lett.* **1996**, *256*, 595.

[34] Nguyen, M. T.; Creve, S.; Vanquickenborne, L. G. *J. Chem. Phys.* **1996**, *105*, 1922.

[35] Lynch, B. J.; Fast, P. L.; Harris, M.; Truhlar, D. G. *J. Phys. Chem. A* **2000,** *104*, 4811.

[36] Tozer, D. J.; Handy, N. C. *J. Phys. Chem. A* **1998,** *102*, 3162.

[37] Hamprecht, F. A.; Cohen, A. J.; Tozer, D. J.; Handy, N. C. *J. Chem. Phys.* **1998**, *109*, 6264.

[38] Sodupe, M.; Bertrán, J.; Rodríguez-Santiago, L.; Baerends, E. J. *J. Phys. Chem. A* **1999,** *103*, 166.

[39] Fast, P. L.; Corchado, J. C.; Sánchez, M. L.; Truhlar, D. G. *J. Phys. Chem. A* **1999,** *103*, 3139.

[40] Petersson, G. A. *ACS Symp. Ser.* **1998**, *677*, 237.

[41] Martin, J. M. L. ACS Symp. Ser. **1998,** *677*, 212.

[42] Blomberg, M. R. A.; Siegbahn, P. E. M. ACS Symp. Ser. **1998,** *677*, 197.

[43] Fast, P. L.; Sánchez, M. L. ; Truhlar, D. G. *J. Chem. Phys.* **1999**, *111*, 2921.

[44] Tratz, C. M.; Fast, P. L.; Truhlar, D. G. *PhysChemComm.* **1999,** *2*, article 14.

[45] Fast, P.L.; Corchado, J.C.; Sánchez, M. L.; Truhlar, D.G. *J. Phys. Chem A* **1999***, 103*, 5129.

[46] Fast, P. L.; Sánchez, M. L.; Corchado, J. C.; Truhlar, D. G. *J. Chem. Phys.* **1999,** *110*, 11679.

[47] Pople, J. A. ; Head-Gordon, M.; Raghavachari, K. *J. Chem. Phys.* **1987**, *87*, 5968.

[48] (a) Ruscic, B.; Feller, D.; Dixon, D. A.; Peterson, K. A.; Harding, L. B.; Asher, R. L.; Wagner, A. F. *J. Phys. Chem. A* **2001**, *105*, 1; (b) Ruscic, B.;Wagner, A. F.; Harding, L. B.; Asher, R. L.; Feller, D.; Dixon, D. A.; Peterson, K. A.; Song, Y.; Qian, X.; Ng, Ch. -Y.; Liu, J.; Chen, W.; Schwenke, D. *J. Phys. Chem. A* **2002**, *106*, 2727.

[49] Herbon, J. T.; Hanson, R. K.; Golden, D. M.; Bowman, C. T. submitted to 29th International Symposium on Combustion, Hokkaido, Japan, July 21-26, 2002.

[50] Joens, J. A. *J. Phys. Chem. A* **2001**, *105*, 11041.

[51] This experimental reaction enthalpy should be revised using new experimental[48-50] and theoretical[48] values for the OH enthalpy of formation.

[52] Bott, J. F.; Cohen, N. *Int. J. Chem. Kinet.* **1991**, *23*, 1017.

[53] Truhlar, D. G.; Garrett, B. C. *J. Am. Chem. Soc.* **1989**, *111*, 1232.

[54] Masgrau, L.; González-Lafont, A.; Lluch, J. M. *Chem. Phys. Lett.* **2002**, *353*, 154.

[55] Smith, I. W. M. ; Ravishankara, A. R. *J. Phys. Chem. A* **2002**, *106*, 4798.

Figure 1. Stationary-point structures for the acetone + OH reaction.
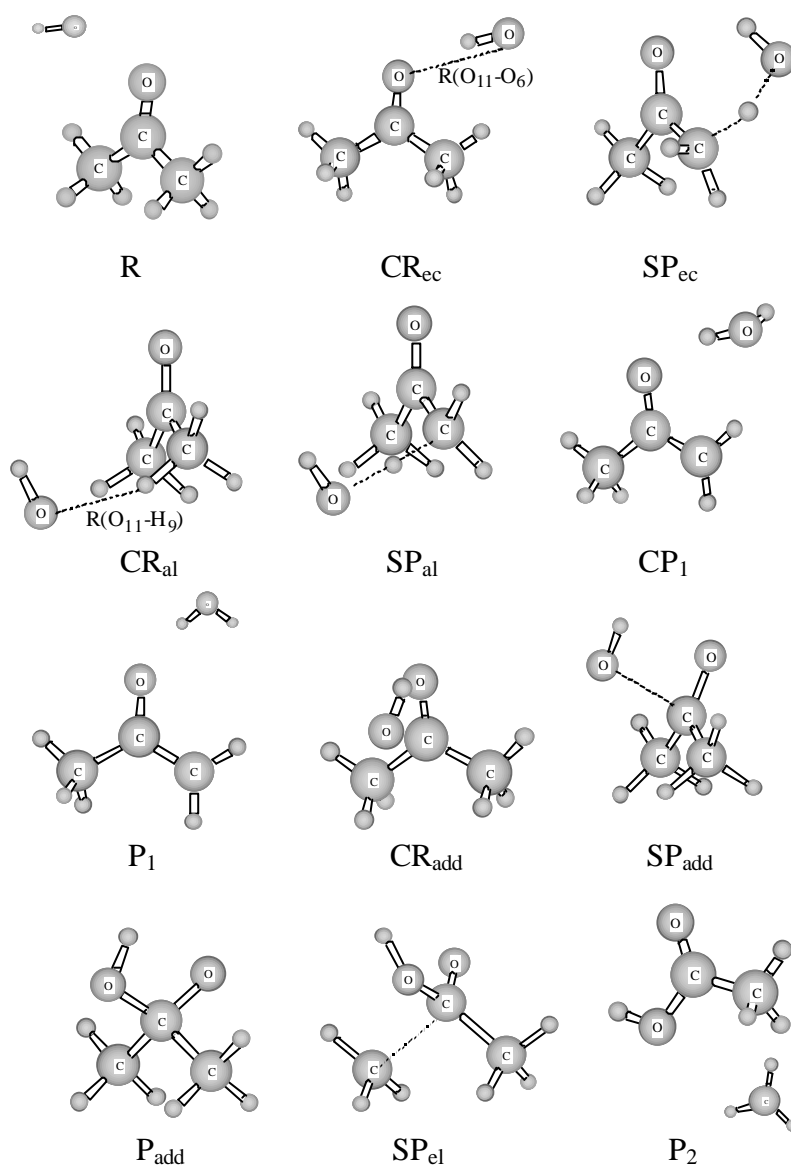
Figure 2. Scheme of the adiabatic ground-sate energy (classical potential energy + ZPE corrections) for the acetone + OH reaction. Three different pathways are depicted: abstraction of a hydrogen eclipsed to the carbonyl group (dash-dot), abstraction of a hydrogen alternated to the carbonyl group (dotted), and addition-elimination (dashed).
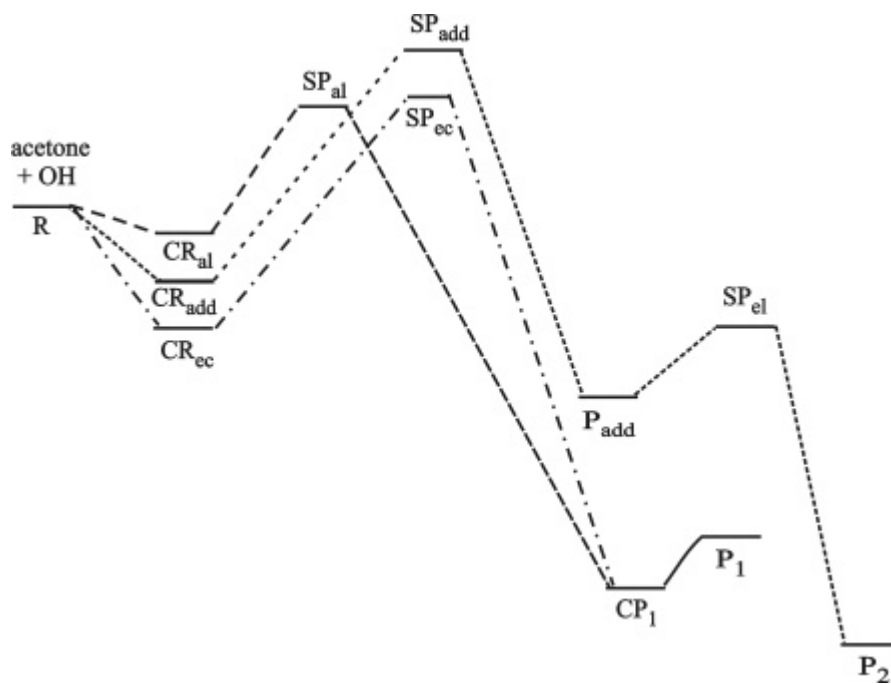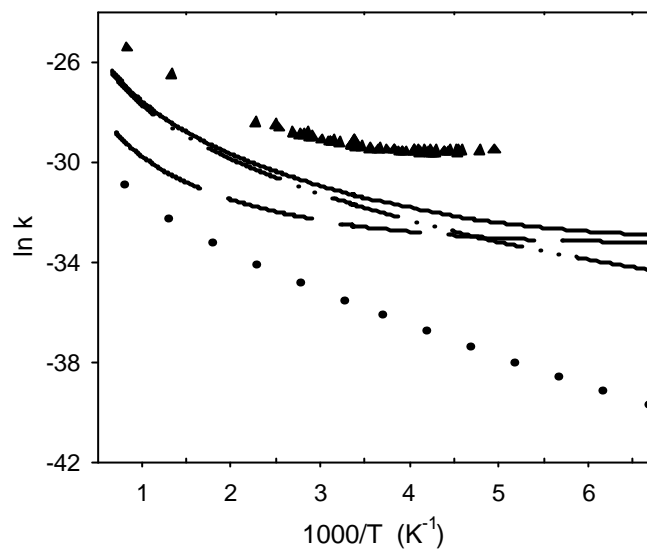
Figure 3. Arrhenius plots for the CBS-RAD(B,B) rate constants (in $cm^3 molecule^{-1} s^{-1}$): overall acetone + OH reaction, k^{CCUS} (solid line), eclipsed pathway, k^{EC} (dashed line), alternated pathway, k^{AL} (dash-dot-dot), and addition elimination pathway, k^{ADD-EL} (dotted). The triangles are for the experimental data.

Figure 4. Arrhenius plots for the B3LYP/6-31G(d) rate constants (in $cm^3 molecule^{-1}s^{-1}$): overall acetone + OH reaction (solid line), eclipsed pathway (dashed line), and alternated pathway (dash-dot-dot). The triangles are for the experimental data.

Table 1. B3LYP/6-31G(d) and CBS-RAD(B,B) energetics (in kcal/mol) for the different regions described in the acetone + OH react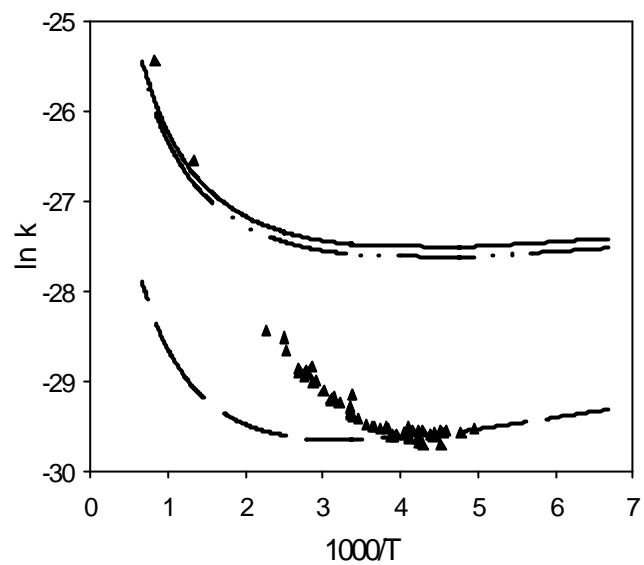ion. From left to right: classical potential and adiabatic energy of reaction for the region; classical potential energy at the B3LYP saddle point structure; s value at the classical potential energy maximum; CBS-RAD (classical) energy barrier height; adiabatic energy at the classical potential energy maximum; s value at the adiabatic energy maximum; adiabatic energy barrier height. All energies are relative to reactants. The s values are in bohr.

B3LYP/6-31G(d)

	ΔV	ΔV_a^G	$V(s=0)$	$s\,(V_{max})$	V_{max}	$V_a^G\,(V_{max})$	$s\,(V^{AG})$	V^{AG}
Eclipsed association	-9.70	-7.55	--	--	--	--	--	--
Eclipsed abstraction	-24.95	-22.89	0.69	--	--	-0.52	-0.24	0.29
Alternated association	-2.46	-1.62	--	--	--	--	--	--
Alternated abstraction	-24.95	-22.89	0.40	--	--	-1.08	-0.42	0.009
Dissociation	-15.57	-15.95	--	--	--	--	--	--
Addition association	-4.40	-3.26	--	--	--	--	--	--
Addition	-21.53	-17.71	-0.39	--	--	1.86	0.08	1.87
Elimination	-25.68	-25.66	-12.58	--	--	-10.04	-0.4	-9.98

CBS-RAD(B,B)

	ΔV	ΔV_a^G	$V(s=0)$	$s\,(V_{max})$	V_{max}	$V_a^G\,(V_{max})$	$s\,(V^{AG})$	V^{AG}
Eclipsed association	-6.82	-4.67	--	--	--	--	--	--
Eclipsed abstraction	-29.25	-27.23	2.02	-0.13	2.60	1.92	-0.24	2.86
Alternated association	-1.69	-0.88	--	--	--	--	--	--
Alternated abstraction	-29.25	-27.23	2.63	-0.14	2.98	2.33	-0.42	2.85
Dissociation	-22.64	-23.02	--	--	--	--	--	--
Addition association	-4.49	-3.35	--	--	--	--	--	--
Addition	-20.38	-16.56	0.92	0.10	0.94	3.21	0.16	3.29
Elimination	-29.25	-29.23	-12.20	-0.20	-12.10	-9.51	-0.28	-9.50

Table 2. Rate constants in $cm^3molecule^{-1}s^{-1}$ (power of 10 in parentheses) for the eclipsed association and the eclipsed abstraction regions, calculated at the CBS-RAD(B,B) electronic level.

T (K)	Eclipsed association	Eclipsed abstraction		
		$k^{TST}(T)$	$k^{CVT}(T)$	$k^{CVT/SCT}(T)$
150	6.05(-10)	4.92(-16)	2.29(-17)	3.74(-15)
175	4.16(-10)	1.10(-15)	7.61(-17)	3.96(-15)
202	2.80(-10)	2.11(-15)	2.00(-16)	4.40(-15)
210	2.55(-10)	2.48(-15)	2.54(-16)	4.56(-15)
220	2.30(-10)	2.99(-15)	3.34(-16)	4.79(-15)
280	1.50(-10)	7.17(-15)	1.18(-15)	6.60(-15)
298	1.37(-10)	8.80(-15)	1.58(-15)	7.33(-15)
300	1.36(-10)	8.99(-15)	1.63(-15)	7.41(-15)
348	1.14(-10)	1.42(-14)	3.07(-15)	9.66(-15)
395	1.02(-10)	2.06(-14)	5.04(-15)	1.24(-14)
400	1.01(-10)	2.14(-14)	5.28(-15)	1.27(-14)
440	9.51(-11)	2.80(-14)	7.48(-15)	1.55(-14)
500	9.00(-11)	3.98(-14)	1.17(-14)	2.05(-14)
600	8.79(-11)	6.55(-14)	2.12(-14)	3.14(-14)
700	8.97(-11)	9.97(-14)	3.44(-14)	4.57(-14)
800	--	1.44(-13)	5.16(-14)	6.41(-14)
1000	--	2.66(-13)	1.00(-13)	1.15(-13)
1200	--	4.44(-13)	1.72(-13)	1.88(-13)
1217	--	4.62(-13)	1.79(-13)	1.95(-13)
1500	--	8.33(-13)	3.28(-13)	3.47(-13)

Table 3. Rate constants in cm^3molecule^{-1}s^{-1} (power of 10 in parentheses) for the alternated abstraction region, calculated at the CBS-RAD(B,B) electronic level.

T (K)	Alternated abstraction		
	$k^{TST}(T)$	$k^{CVT}(T)$	$k^{CVT/SCT}(T)$
150	2.94(-16)	8.37(-17)	1.25(-15)
175	8.70(-16)	3.08(-16)	2.24(-15)
202	2.10(-15)	8.89(-16)	3.90(-15)
210	2.62(-15)	1.16(-15)	4.54(-15)
220	3.39(-15)	1.57(-15)	5.45(-15)
280	1.11(-14)	6.47(-15)	1.37(-14)
298	1.46(-14)	8.95(-15)	1.73(-14)
300	1.51(-14)	9.26(-15)	1.77(-14)
348	2.78(-14)	1.90(-14)	3.03(-14)
395	4.51(-14)	3.32(-14)	4.71(-14)
400	4.73(-14)	3.50(-14)	4.91(-14)
440	6.68(-14)	5.19(-14)	6.78(-14)
500	1.04(-13)	8.55(-14)	1.03(-13)
600	1.91(-13)	1.67(-13)	1.85(-13)
700	3.14(-13)	2.84(-13)	2.99(-13)
800	4.78(-13)	4.43(-13)	4.51(-13)
1000	9.56(-13)	9.11(-13)	8.94(-13)
1200	1.67(-12)	1.61(-12)	1.56(-12)
1217	1.74(-12)	1.68(-12)	1.63(-12)
1500	3.29(-12)	3.20(-12)	3.09(-12)

Table 4. Rate constants in $cm^3 molecule^{-1}s^{-1}$ (power of 10 in parentheses) for the addition and the elimination regions, calculated at the CBS-RAD(B,B) electronic level.

T (K)	Addition			Elimination	
	$k^{TST}(T)$	$k^{CVT}(T)$	$k^{CVT/SCT}(T)$	$k^{TST}(T)$	$k^{CVT}(T)$
150	2.62(-18)	2.48(-18)	5.88(-18)	1.54(-01)	7.41(+00)
175	9.84(-18)	9.33(-18)	1.69(-17)	1.13(-01)	5.96(-02)
202	2.86(-17)	2.70(-17)	4.15(-17)	2.20(-03)	1.24(-03)
210	3.72(-17)	3.52(-17)	5.22(-17)	8.33(-04)	4.77(-04)
220	5.05(-17)	4.78(-17)	6.80(-17)	2.73(-04)	1.59(-04)
280	2.05(-16)	1.93(-16)	2.37(-16)	1.84(-06)	1.17(-06)
298	2.83(-16)	2.65(-16)	3.16(-16)	6.14(-07)	3.95(-07)
300	2.92(-16)	2.74(-16)	3.26(-16)	5.48(-07)	3.54(-07)
348	5.91(-16)	5.52(-16)	6.22(-16)	5.38(-08)	3.60(-08)
395	1.02(-15)	9.50(-16)	1.03(-15)	9.84(-09)	6.73(-09)
400	1.08(-15)	1.00(-15)	1.08(-15)	8.42(-09)	5.77(-09)
440	1.58(-15)	1.46(-15)	1.55(-15)	2.78(-09)	1.93(-09)
500	2.58(-15)	2.36(-15)	2.44(-15)	7.54(-10)	5.32(-10)
600	4.93(-15)	4.45(-15)	4.47(-15)	1.62(-10)	1.16(-10)
700	8.24(-15)	7.36(-15)	7.23(-15)	5.72(-11)	4.14(-11)
800	1.26(-14)	1.11(-14)	1.08(-14)	2.73(-11)	1.99(-11)
1000	2.50(-14)	2.16(-14)	2.04(-14)	1.06(-11)	7.73(-12)
1200	4.28(-14)	3.61(-14)	3.34(-14)	6.13(-12)	4.46(-12)
1217	4.45(-14)	3.75(-14)	3.47(-14)	5.92(-12)	4.30(-12)
1500	8.07(-14)	6.61(-14)	5.99(-14)	3.91(-12)	2.83(-12)

Table 5. Rate constants in $cm^3 molecule^{-1}s^{-1}$ (power of 10 in parentheses) calculated at the CBS-RAD(B,B) level. From left to right: overall eclipsed abstraction mechanism; overall alternated abstraction mechanism; addition-elimination mechanism; overall acetone + OH reaction. The last column corresponds to experimental data.

T (K)	$k^{EC}(T)$	$k^{AL}(T)$	$k^{ADD-EL}(T)$	Acetone + OH $k^{CCUS}(T)$	Experimental
150	3.74(-15)	1.25(-15)	5.88(-18)	5.00(-15)	--
175	3.96(-15)	2.24(-15)	1.69(-17)	6.22(-15)	--
202	4.40(-15)	3.90(-15)	4.15(-17)	8.34(-15)	1.48 (-13)[a]
210	4.56(-15)	4.54(-15)	5.22(-17)	9.15(-15)	1.44 (-13)[b]
220	4.79(-15)	5.45(-15)	6.80(-17)	1.03(-14)	1.43 (-13)[a]
280	6.60(-15)	1.37(-14)	2.37(-16)	2.06(-14)	1.56 (-13)[b]
298	7.33(-15)	1.73(-14)	3.16(-16)	2.49(-14)	1.77 (-13)[a]
300	7.41(-15)	1.77(-14)	3.26(-16)	2.54(-14)	1.78 (-13)[b]
348	9.66(-15)	3.03(-14)	6.22(-16)	4.06(-14)	2.49 (-13)[c]
395	1.24(-14)	4.71(-14)	1.03(-15)	6.05(-14)	3.54 (-13)[a]
400	1.27(-14)	4.91(-14)	1.08(-15)	6.29(-14)	4.07 (-13)[d]
440	1.55(-14)	6.78(-14)	1.55(-15)	8.48(-14)	4.36 (-13)[d]
500	2.05(-14)	1.03(-13)	2.44(-15)	1.26(-13)	
600	3.14(-14)	1.85(-13)	4.47(-15)	2.21(-13)	
700	4.57(-14)	2.99(-13)	7.23(-15)	3.52(-13)	2.92 (-12)[e]
800	6.41(-14)	4.51(-13)	1.08(-14)	5.26(-13)	
1000	1.15(-13)	8.94(-13)	2.03(-14)	1.03(-12)	
1200	1.88(-13)	1.56(-12)	3.32(-14)	1.78(-12)	
1217	1.95(-13)	1.63(-12)	3.44(-14)	1.86(-12)	8.8 (-12)[f]
1500	3.47(-13)	3.09(-12)	5.87(-14)	3.50(-12)	

[a] From Ref. X (Crowley and coworkers)
[b] From the fitting in Ref. X (Crowley and coworkers)
[c] From Ref. X (Mellouki)
[d] From Ref. X (Kurylo)
[e] From Ref. X, measured at 753 K (Tranter and Walker)
[f] From Ref. X (Bott and Cohen, ref 12 de Mellouki)

Table 6. Quasi-thermodynamic activation enthalpy (in kcal/mol) and entropy (cal/mol K) for the eclipsed abstraction, the alternated abstraction and the addition pathways, at 202 and 1000 K. The generalized (^{GT}) and the total (^{TOT}) values for these magnitudes are given (see part D of the Results and Discussion section for details).

	202 K				1000 K			
	$\Delta H^{GT}(s_*)$	$\Delta S^{GT}(s_*)$	ΔH^{TOT}	ΔS^{TOT}	$\Delta H^{GT}(s_*)$	$\Delta S^{GT}(s_*)$	ΔH^{TOT}	ΔS^{TOT}
Eclipsed abstraction	1.72	-26.04	-0.44	-30.57	1.89	-23.46	1.30	-23.78
Alternated abstraction	1.98	-21.76	0.77	-24.84	2.33	-18.63	2.11	-18.89
Addition	1.98	-28.71	1.59	-29.79	1.74	-26.67	1.54	-26.98

Table 7. CBS-RAD(B,B) branching ratio (in %) for the addition-elimination pathway at different temperatures.

T (K)	$k^{\text{ADD-EL}}/k^{\text{CCUS}}$	T (K)	$k^{\text{ADD-EL}}/k^{\text{CCUS}}$
150	0.12	400	1.72
175	0.27	440	1.83
202	0.50	500	1.94
210	0.57	600	2.02
220	0.66	700	2.05
280	1.15	800	2.05
298	1.27	1000	1.98
300	1.28	1200	1.86
348	1.53	1217	1.85
395	1.70	1500	1.68